Comprehensive plasma lipidomic profiles reveal a lipid-based signature panel as a diagnostic and predictive biomarker for cerebral aneurysms

Yong-Dong Li (dr_liyongdong@sina.com)
Shanghai Jiao Tong University Affiliated Sixth People's Hospital, Shanghai, China
Yue-Qi Zhu
Shanghai Jiao Tong University Affiliated Sixth People's Hospital, Shanghai, China
Bing Zhao
Renji Hospital, Shanghai Jiao Tong University, School of Medicine
Yu He
Shanghai Jiao Tong University Affiliated Sixth People's Hospital
Bin-Xian Gu
Shanghai Jiao Tong University Affiliated Sixth People's Hospital
Hao-Tao Lu
Shanghai Jiao Tong University Affiliated Sixth People's Hospital
Yi Gu
Shanghai Jiao Tong University Affiliated Sixth People's Hospital
Li-Ming Wei
Shanghai Jiao Tong University Affiliated Sixth People's Hospital
Yao-Hua Pan
Renji Hospital, Shanghai Jiao Tong University, School of Medicine
Zheng-Nong Chen
Shanghai Jiao Tong University Affiliated Sixth People's Hospital
Yong-Ning Sun
Shanghai Jiao Tong University Affiliated Sixth People's Hospital
Wu Wang
Shanghai Jiao Tong University Affiliated Sixth People's Hospital

Article

Keywords: Cerebral aneurysm, lipidomics, liquid chromatography–mass spectrometry, triglyceride, non-negative matrix factorization

Posted Date: April 1st, 2021

DOI: https://doi.org/10.21203/rs.3.rs-228632/v1

Abstract

We investigated lipidomic features from healthy controls (HCs), patients with unruptured cerebral aneurysms (UCAs) and ruptured CAs (RCAs) to analyze their lipidomic profiles and identify a lipid signature associated with CAs. Patients (n = 540) were enrolled from two centers. We identified significantly altered plasma lipids in 2 cohort with the total lipid intensity decreasing from HC to UCA to RCA. Triglycerides comprised the distinct profile of lipids in CAs. A four-lipid signatures showed good calibration and diagnostic prediction for CA *vs*. HC and UCA *vs*. RCA, but independent discriminate CA from HC, UCA from RCA, and RCA (RI and RII) or UCA (UI and UII) subtypes, in training and validation cohorts. Comprehensive lipidomic profiles identified decreased lipids as a prominent feature of CA development, and a four-lipid signature could not only better diagnose and predict UCAs/RCAs from HCs, but also predicted patients subtypes with severe RCA or high-risk UCA.

Introduction

Cerebral aneurysms (CAs), defined as abnormal focal dilatations of a cerebral artery with attenuation of the vessel wall, are common vascular lesions, with a prevalence of 1–7% in adults and an annual rupture rate of 0–1% [1–6]. Although most CAs are small and remain asymptomatic, ruptured CAs (RCAs), the most common cause of non-traumatic subarachnoid hemorrhage (SAH), can be catastrophic, with a mortality rate of 25–50% and permanent disability in nearly 50% of survivors [2–5].

Recent studies have shown that CA formation does not necessarily progress to an RCA, and CA development appears to be a distinct process from CA rupture [7]. The histology of the walls of intact and ruptured CAs are different [8–10]. Characteristically, ruptured CAs have a degenerated and decellularized matrix with increased complement system activation, antibody accumulation, and inflammatory cell infiltration [8–10]. By contrast, intact CA walls frequently resemble the normal arterial intima, or, following mechanical injury or hypertension development, the intima becomes hyperplastic [9, 11]. In intact CAs, the underlying mechanisms of mural smooth muscle cell (SMC) loss and increased infiltration of inflammatory cells into the neointima-like (or intima-like) CA wall remain to be determined.

CA wall degeneration and the likelihood of rupture may be related to lipid oxidation and accumulation, because they might trigger SMC-derived foam cell formation, inflammation, mural SMCs loss, and degenerative CA wall remodeling, eventually leading to wall rupture [7,12–15]. Research has demonstrated that the lipid accumulation pattern, associated with mural SMC loss and wall degeneration, is different between unruptured and ruptured CAs [13,14]. However, the mechanism of lipid accumulation remains unknown.

Although lipid accumulation was observed in CA walls, plasma total cholesterol and triglyceride (TG) levels were often normal [13,14]. In addition, there are insufficient aneurismal tissues for clinical study, because they are difficult to obtain, especially for a large number of cases. Moreover, the lipid alterations in CA walls do not explain the complexity of patients with CA systemically. Recent developments in

lipidomic technologies have provided new insights into this complex area. Plasma lipid species and classes/subclasses have been identified as associated with type 2 diabetes mellitus (T2DM) [16] and cardiovascular diseases (CVDs) [17,18], suggesting that these lipid species might be useful biomarkers for these diseases. However, to the best of our knowledge, no studies have investigated the plasma lipid profile and biomarkers associated with CAs.

Accordingly, we performed an untargeted lipidomics evaluation using the plasma from HCs, patients with UCAs, and those with RCAs, to identify a plasma lipid profile for patients with CA using a LC-MS platform in a large case-control study.
First, we analyzed the lipidomic profiles comprehensively in the three groups and reported an in-depth analysis of the plasma lipid alterations that could be used to differentiate among them. Subsequently, we built a four-lipid biomarker signature that could not only diagnose and predict UCAs/RCAs, but also predicted subtype patients with severe RCA or high-risk UCA.

Results

Baseline characteristics

The brief study designs are shown in **Fig.1, A-B**. The study first recruited 360 patients (cohort 1, 144 men and 216 women, median age: 55.5 years; age range: 17–87 years), including 120 HCs, 120 patients with UCA, and 120 age- and sex-matched patients with RCA. The baseline characteristics of the human subjects in the three groups, based on their diagnostic status, are shown in **Extended Data 1 T*able S1***. There were no significant differences in sex, age, hypertension, diabetes mellitus, hyperlipemia, coronary heart disease, smoking, alcohol consumption, and body mass index (BMI) among the three groups of participants. The duration of plasma storage at measurement did not differ among the three groups. There were 147 aneurysms in the 120 patients with UCA and 145 aneurysms in the 120 patients with RCA.

Next, we enrolled 72 men and 108 women for trend testing of the primary results from the 180 patients (cohort 2), including 60 HCs, 60 patients with UCA, and 60 age- and sex-matched patients with RCA. Baseline characteristics of the human subjects in the three groups are shown in **Extended Data 2 *Table S1*.**

Overview of the distribution of lipid species and subclass intensities in the three groups

To enable comprehensive plasma lipidomic profiling of CAs, lipidomic analysis was performed with an untargeted LC-MS method using a CSH C18 column and using the same LC-MS with consistent quality control in a total of 360 participants from one center and 68 QC samples (**Extended Data 1 Fig. S1**).

After QC and support vector regression (SVR), LC-MS detected 1312 lipids (972 ESI+ and 340 ESI-) covering 8 lipid categories and 29 subclasses in all three groups, in which TG was the most abundant lipid in all three groups, followed by phosphatidylcholine (PC), sphingomyelin (SM), phosphatidylethano-

lamine (PE), and ceramides (Cer) **(Fig.2 A**). In the UCA and RCA samples, the numbers of identified lipids were the same as those identified in the HC samples after case-by-case review. We then performed PCA to analyze the lipid data set and identify the characteristics of each group. QC samples, shown as calamus ellipses, were center clustered, which indicated good reproducibility of the instruments and stability during the lipidomics study (**Fig. 2B**).

The lipid intensity of every sample accompanied by sex and age is shown in **Fig. 2 C**. The total lipid intensity comparisons of the three groups, with and without sex and/or age data, is shown in **Fig. 2 D-I**. The trend of total lipid intensity decreased from HC to UCA to RCA, and a significant difference among the three groups was observed (**Fig. 2 D**, ANOVA test, $p < 0.001$). The same decreased trend was also observed in the F (female) or M (male) subgroups (**Fig. 2 G,** ANOVA test, $p < 0.001$) and age subgroups (**Fig. 2 I,** ANOVA test, $p < 0.05$) among the three groups. There were no significant differences between M and F in each of the three groups (**Fig. 2 E**), among the four age subgroups in each of the three groups (**Fig. 2 F**), and among the four age subgroups in the F or M subgroups (**Fig. 2 H**). In addition, the same decreased trend was observed in 26 of the 29 subclasses among the three groups (**Fig. 2 J,** ANOVA test, $p < 0.05$).

The same trend was well tested in cohort 2 (**Extended Data 2 and Extended Data 2 Fig. S2**.)

Plasma lipidomic profiling of HCs, UCAs, and RCAs

To investigate the lipidomic changes associated with CAs, three paired comparisons were performed. The differential lipids that satisfied the criterion of variable importance in the projection (VIP) of > 1.0 and *p* value < 0.05 were considered as potential differential lipids. An Orthogonal partial least squares discriminant analysis (OPLS-DA) model was employed to further investigate lipid changes and differential lipids. OPLS-DA score plots revealed that all three groups could be discriminated (**Fig. 3 A-C**). Parameters for the explained variation (R2), an indicator of model robustness, and the cross-validated predictive ability (Q2) were obtained, as shown in **Fig. 3A-C.** The heatmap depicts the relative abundance of all lipids in all three groups (**Fig. 3 D**). Among these three paired comparisons, the lipid profiles of RCA were better distinguished from those of the HC group (**Fig. 3 D**).

As summarized in **Extended Data 1** ***Table S2-3***, 75 and 130 differential lipids were identified from the comparisons of UCA *vs*. HC and RCA *vs*. HC participants, respectively. Compared with the HC group, 5.5% (75) of the identified lipids were significantly different in the UCA group (*p* value < 0.05; VIP > 1.0), while, 9.9% (130) of identified lipids were significantly altered in the RCA group (*p* value < 0.05; VIP > 1.0), and the number of altered lipids were greater in the RCA group than in the UCA group (c2 test, $p < 0.05$). From this trend, we found that the number of altered lipids correlated positively with the severity of the clinical CA status (UCA and RCA). We hypothesized that increased lipid alteration in patients with a CA resulted in increased likelihood of CA rupture.

Interestingly, compared with HCs, except for 10 lipids in UCA group, the other altered lipids were under-represented, with lower levels in the UCA and RCA groups (**Extended Data 1** ***Table S2-3***). This indicated

that most altered lipids were decreased in the plasma of the CA group, and the degree of the decreased lipids was much lower in the RCA group than that in UCA the group. Using a combination of our results and published research (13,14), we hypothesized that the decreased lipids in plasma probably accumulated in the CA and normal artery wall, which resulted in the formation, development, and rupture of CAs. This trend was also tested in cohort 2 (**Extended Data 2 and Extended Data 2 Fig. S3)**.

In addition, as shown in **Extended Data 1** ***Tables S2-5***, there were 35 differential lipids including 4 lipid subclasses (1 LPC, 4 SMs, 7 PCs, and 23 TGs) that were significantly altered among the three groups (**Fig. 3E**), which could be used as potential biomarkers to diagnose or to discriminate CAs from HCs. The relative levels of these 35 differential lipid profiles were presented as a heatmap and a differential lipid profile was observed when comparing UCA to HC, RCA to HC, and RCA to UCA (**Fig. 3 F)**. The lipids exhibited the same decreasing trends from HC to UCA to RCA, and a significant difference was observed among the three groups and between each of the two groups (**Fig. 3 G**, $p < 0.001$).

TGs were the distinct profile of lipids in patients with UCA and RCA as compared with HCs

The large number of samples in our cohort allowed us to investigate the association between lipids shifts and CA development according to clinical classification (UCA and RCA). As shown in **Extended Data 1** ***Table S2*** and **Fig. 4 A**, 75 differential lipids were identified from the comparisons of UCA vs HC, of which, 65 were downregulated and 10 were upregulated. 13 out of 75 altered lipids were significantly decreased (Fold change (FC) < 0.75 or log2FC < -0.42) and no lipids were significantly increased (FC > 1.5 or log2FC > 0.59) in patients with UCA compared with HCs **Extended Data 1** ***Table S2*** and **Fig. 4 A**). Of the 13 significantly decreased lipids, all were TGs. Furthermore, the 9 significantly decreased lipids including TG(56:2)+NH4, TG(54:1)+NH4, TG(52:0)+NH4, TG(54:2)+NH4, TG(56:4)+NH4, TG(56:5)+NH4, TG(53:2)+NH4, TG(53:3)+NH4 and TG(54:3)+NH4 were further decreased in patients with RCA as compared with HCs.

In patients with RCAs, all the differential lipids were decreased as compared with HCs (**Extended Data 1** ***Table S3*** **and Fig.4B**). 75 out of 130 altered lipids were significantly decreased (FC< 0.75 or log2FC < -0.42), and 24 lipids showed a less than 0.5-fold decrease (log2FC < -1). Of the 75 significantly decreased lipids, 86.7% (65/75) were TGs, and all the 24 lipids with a less than 0.5-fold decrease were TGs (**Extended Data 1** ***Table S3*****, and Fig.4B**). Therefore, although there were many lipids altered from UCA to RCA, we only identified one distinct lipid subclass (TGs) with respect to clinical classification.

In addition, as shown in **Extended Data 1** ***Table S4*** **and Fig.4C**, there were 119 identifiable lipids exhibiting statistically significant differential abundance between RCAs and UCAs, and the majorities (115 lipids) were decreased in RCAs as compared with UCAs. Of these, 46 out of 119 altered lipids were significantly decreased (FC< 0.75 or log2FC < -0.42) and 16 lipids showed a less than 0.5-fold decrease (log2FC < -1). Of the 46 significantly decreased lipids, 95.7% (44/46) were TGs, and all the 16 lipids were TGs (**Extended Data 1** ***Table S4*** **and Fig.4C**). Of note, as compared with HCs, we observed that TG became the predominant and distinct profile of altered lipid, which indicated that TG metabolism was severely disrupted in patients with CAs.

In addition, TGs were also the distinct profile of lipids in patients with UCA and RCA as compared with HCs in cohort 2 **(Extended Data 2 and Extended Data 2 Fig. 4**.)

Lipid-based diagnostic prediction model for CA *vs*. HC

To investigate the lipid-based diagnostic prediction model for CAs (UCAs + RCAs), we first discriminated CAs from HCs, and then differentiated UCAs from RCAs. We assigned cohort 1 (n = 360; HCs = 120, CAs = 240) to the training cohort, and cohort 2 (n = 180; HCs = 60, CAs =120) to the validation cohort. Therefore, the ratio of samples in the training and validation sets was 2:1. The baseline characteristics of subjects in the two cohorts are shown in **Extended Data 1 Table S6**.

To discriminate CAs from HCs, the two cohorts were subjected to an independent and comprehensive analysis to discover biomarkers. First, the lipid profiles between the HCs and the patients with CAs were compared in the two cohorts, which identified 61 differentially abundant (variable importance in projection (VIP) of > 1.0 and p value < 0.05) candidates in both cohorts. Secondly, we used random forest algorithms and the least absolute shrinkage and selection operator (LASSO) to decrease the number of lipid biomarkers, which produced 12 overlapping biomarkers from the two algorithms.

To make the model concise and consistent, we selected four lipids (PE(20:1p/18:2)+H, CerG1(d40:4)+NH4, TG (18:0p/16:0/16:1)+NH4, and TG (54:2e)+NH4) that exhibited consistent differential abundance in the UCA *vs*. RCA groups as our final biomarker. Then, we constructed a nomogram (**Fig. 5A**) and a diagnostic prediction score (dp-score) that was obtained according to the coefficients from generalized linear models (regressions) (**Extended Data 1** ***Table S7***). The risk score model was developed as follows: 0.6243+ (-0.4460*PE (20:1p/18:2)+H) + (-0.3263* CerG1(d40:4)+NH4) + (-0.5968* TG(18:0p/16:0/16:1)+NH4) + (-1.2855* TG(54:2e)+NH4).

First, the training cohort was used to train the 4-lipid prediction model. In the training cohort, the nomogram's calibration plot demonstrated good agreement between observation and prediction (**Fig. 5B**). The Hosmer-Lemeshow (HL) test statistic was not significant (P = 0.244), indicating a good fit to the model. The receiver operator characteristic (ROC) analysis for the nomogram of the four biomarkers yielded areas under the ROC curve (AUCs) of 0.814 (95% confidence interval (CI): 0.767–0.861, **Fig. 5 C, D**) for the training cohort. The dp-score showed specificity and sensitivity of 60.0% and 87.5, respectively (**Fig. 5D**), using the best cutoff value.

Next, the four-lipid signature and the same statistical model were applied in the validation cohort (60 HC and 120 CA cases) to assess the accuracy of the signature. In the validation cohort, the lipid biomarkers showed excellent diagnostic accuracy to the identify patients with CAs. As it did in the training cohort, the nomogram showed favorable calibration in the validation cohort (**Fig. 5E**). The HL test result was not significant (p = 0.387), and in the validation cohort, the AUCs were 0.803 (95% CI: 0.735–0.871, **Fig. 5F, G**) for the nomogram. The specificity and sensitivity of the dp-score were 85 % and 69.2%, respectively (**Fig. 5G**).

Next, decision curve analysis (DCA) was used to compare the lipid performance of the model in the training and validation cohorts. To diagnose CAs in the validation and training cohorts, the developed model showed the highest net benefit within the ranges of most of the potential thresholds (**Fig. 5H**). Based on the lipid nomogram, the net benefits were similar, with several overlaps, within this range. This suggested the possibility of using the nomogram in clinical practice for the diagnosis and prediction of CAs.

A lipid-based combination diagnostic prediction model for CA *vs*. HC

Sex, age, and hypertension are known to be associated with CAs; therefore, whether a model combining our lipid signature with these three preoperative clinical features could improve the diagnostic accuracy to detect CA in clinic was assessed. The results showed that the diagnostic accuracy for CA of the combined signature was slightly better in both the validation and training cohorts (AUC values of 0.802 and 0.836, respectively, **Fig. 5 I, J, and Extended Data 1 Fig. S2**). Moreover, compared with the preoperative clinical features alone, including gender, age and hypertension, the combination signature demonstrated significantly improved diagnostic accuracy. Finally, using the cutoffs determined using the Youden index from this four-lipid signature model, all patients were categorized into high- and low-risk groups. The univariate and multivariate logistic regression analyses results are shown in **Extended Data 1 *Table S8***. In both clinical cohorts, multivariate analysis showed that the four-lipid signature was an independent predictor to discriminate CAs from HCs, (training cohort: odds ratio [OR], 10.13; 95% CI, 5.93–17.74; p < 0 .001; validation cohort: OR, 12.66; 95% CI, 5.84–30.28, p < 0.001, **Extended Data 1 *Table S8***).

Lipid-based diagnostic prediction model for UCA *vs*. RCA

To differentiate UCAs from RCAs, we assigned cohort 1 (n = 240; UCAs = 120, RCAs = 120) to the training cohort, and cohort 2 (n = 120; UCAs = 60, RCAs = 60) to the validation cohort. The baseline characteristics of cohort 1 and cohort 2 subjects are shown in **Extended Data 1 *Table S9***. Consistent with the model for CAs *vs*. HCs, we still used the four biomarkers as the diagnostic prediction model for UCAs *vs*. RCAs. We constructed a nomogram and a dp-score that was obtained according to the coefficients and the constant derived from multinomial logistic regression (**Extended Data 1 *Table S10***). The risk score model was obtained as follow: -0.0412+ (0.0320*PE (20:1p/18:2)+H) + (-0.7768* CerG1(d40:4)+NH4) +(-0.3816* TG(18:0p/16:0/16:1)+NH4) + (-1.2405* TG(54:2e)+NH) .

Fig. 6A shows the nomogram for UCAs *vs*. RCAs with the four biomarkers. The calibration plot of the nomogram that agreement between observation and prediction agreed well in the validation and training cohorts (**Fig. 6B, E**). The training cohort revealed a calibration slope of 1.0, with a nonsignificant HL test statistic of 0.176, and the test cohorts revealed a calibration slope of 0.744, with a nonsignificant HL test statistic of 0.345. The AUC values for the training and test cohorts were 0.775 (95% CI, 0.699–0.934, **Fig. 6 C, D**) and 0.721 (95% CI, 0.692–0.955, **Fig. 6 F, G**), respectively.

The DCA for the lipid nomogram of UCAs *vs*. RCAs is presented in **Fig. 6 H**. The decision curve indicated that at a threshold probability of 20–85% for a patient or doctor, then using the developed lipid nomogram for the diagnosis and prediction UCAs from RCAs would add more benefit than either the treat-none scheme or the treat-all-patients scheme. The net benefit of the test cohort was somewhat lower than the net benefit of the training cohort based on the lipid nomogram within this range. This suggested possibility of using the nomogram in clinical practice to diagnose and predict UCAs from RCAs

A lipid-based combination diagnostic prediction model for UCAs vs RCAs

To further increase the accuracy of diagnosis of URCs or RCAs in the clinic, we also assessed a combination the three preoperative clinical features and the developed model lipid signature. In the validation and training cohorts, the combination signature demonstrated slightly better diagnostic accuracy for URCs or RCAs (AUCs of 0.719 and 0.78, respectively, **Fig. 6 I, J and Extended Data 1 Fig. S3**). Moreover, in terms of diagnostic accuracy, compared that that of the preoperative clinical features sex, age, and hypertension, the combination signature demonstrated a significant improvement. Finally, using the Youden index-derived cutoffs from the four-lipid signature model, all patients were categorized into high- and low-risk groups. The results of for the univariate and multivariate logistic regression analyses results are shown in **Extended Data 1** ***Table S11***. In both cohorts, multivariate analysis identified the four-lipid signature as an independent predictor to discriminate UCA form RCA (training cohort: OR, 6.44; 95% CI, 3.68–11.56; $p < 0.001$; validation cohort: OR, 4.65; 95% CI, 2.10–10.84, $p < 0.001$, **Extended Data 1** ***Table S11***).

Lipid-based subtyping of RCA

A lower lipid intensity in RCA was associated with patients with severe RCA

To explore the lipid-defined specific subtypes within CA, stratification analysis was carried out using non-negative matrix factorization (NMF) consensus-clustering [19,20]. NMF consensus-clustering was first performed for RCA in cohort 1, and two major lipid subtypes (R-I and R-II) were identified among the RCA samples (**Fig. 7 A**, **Extended Data 1 Fig. S4**), with 65 cases belonging to R-I and 55 belonging to R-II. The total lipid intensity of R-II was significantly lower than that of R-I (**Fig. 7 B**, $p < 0.001$). The relative abundance of the two subtypes according to age, sex, etc., is shown in **Fig. 7C.**

To explore the clinical characteristics between the R-I and R-II subgroups, the baseline characteristics of the subjects in the two subgroups were compared. There were no significant differences in sex, age, hypertension, diabetes mellitus, hyperlipemia, smoking, alcohol consumption, and BMI between R-I and R-II (**Extended Data 1** ***Table S12***). Subsequently, we compared the aneurysm characteristics associated with RCA, such as aneurysm size, location, aneurysm neck, single or multiple, regular or irregular, bifurcation or sidewall aneurysm, modified fisher grade (MFG) [21], Glasgow Coma Scale (GCS), the Coma number at onset, ventricular drainage (VD), and hospital day. There were significant differences in MFG, GCS, and the number of Coma at onset between R-I and R-II **(Fig. 7 D)**; no other significant differences were observed (**Extended Data 1** ***Table S12***). **Fig. 7 E-F** show typical cases in the R-I subtype, and **Fig. 7 G-H**

show typical cases in the R-II subtype. These results indicated that patients in the R-II subgroup were associated with severe RCA.

Diagnostic prediction potential of the four-lipid signature for patients with severe RCA

As mentioned-above, patients in R-II are often associated with severe or poor outcomes in the clinic; therefore, we next evaluated the diagnostic predictive potential of the four-lipid biomarker signature for patients with severe RCA. First, the Youden index-derived cutoffs from the four-lipid signature were used to separate the patients with RCA into high- and low-risk groups, which were then analyzed as independent predictors using univariate and multivariate logistic regression. Multivariate logistic regression analysis identified the four-lipid signature as an independent predictor of detection severe RCA, in the two clinical cohorts (training cohort: OR, 6.46; 95% CI, 2.71–16.55; $p < 0.001$; validation cohort: OR, 4.33; 95% CI, 1.30–16.06, $p = 0.01$, **Extended Data 1** ***Table S13***). Thus, in addition to diagnosing RCA, the four-lipid signature could also predict patients with severe RCA.

Lipid-based subtyping of UCA

UCA subtypes predict slow or rapid aneurysm growth

Next, NMF consensus-clustering was performed for UCA in cohort 1, and two major lipid subtypes (U-I and U-II) were identified among the UCA samples (**Fig. 8A**, **Extended Data 1 Fig. S5**) with 54 belonging to subtype U-I and 66 cases belonging to U-II. The total lipid intensity of U-II was significantly lower than that of U-I (**Fig. 8B**, $p < 0.001$). The relative abundance of the two subtypes by age, sex, and etc., is shown in **Fig. 8C**.

To explore the clinical characteristics between U-I and U-II, the baseline characteristics of the human subjects and the aneurysm characteristics in the two subgroups were compared. However, there were no significant differences in sex, age, hypertension, diabetes mellitus, hyperlipemia, smoking, alcohol consumption, BMI, aneurysm size, location, aneurysm neck, single or multiple, regular or irregular, bifurcation or sidewall, and hospital day between the U-I and U-II subtypes (**Extended Data 1** ***Table S14***).

We next checked the patients using MRA follow-up. Although, most patients with UCAs were treated when detected, we still enrolled 23 UCA patients in this study, among whom 20 were followed-up using MRA for more than seven years. According to NMF consensus-clustering, 10 patients were classified in the U-I subgroup and 10 were in the U-II subgroup. Other than the lipid intensity of U-II being significantly lower than that of U-I, we noticed that seven of ten UCAs (70%) in the U-II subtype were enlarged, while only two of ten UCAs (20%) in the U-I subtype were enlarged. Therefore, the aneurysm growth rate was higher in the U-II than in the U-I subtype (c2 test, $p < 0.05$), which indicated that the lower lipid intensity in the U-II subtype was associated with rapid CA progression, when compared to those in the U-I subtype. **Fig. 8 D-E** show the typical cases in U-I, and **Fig. 8 F-G** show the typical cases in U-II. These illustrated that rapid aneurysm growth in the U-II subtype group increased the chance of CA rupture, while the slow growth

observed in the U-I subtype group might be associated with slower aneurysm progression and resistance to CA rupture.

Diagnostic prediction potential of the four-lipid signature for high-risk patients

Patients in the U-II subtype group are associated with rapid aneurysm growth and the chance of CA rupture; therefore, we next evaluated the diagnostic predictive potential of our lipid biomarkers for patients with UCA with rapid growth. First, the Youden index-derived cutoffs from four-lipid signature model were used to separate the patients with RCA into high- and low-risk groups, which were then assessed as independent predictor using univariate and multivariate logistic regression analyses. In both cohorts, multivariate logistic regression analysis identified the four-lipid signature an independent predictor to detect patients with UCA with rapid growth (training cohort: OR, 6.04; 95% CI, 2.73–14.05; $p < 0.001$; validation cohort: OR, 145.3, 95% CI, 21.3–3203.3, $p < 0.001$, **Extended Data 1** ***Table S15***).

In addition, when we extracted 20 UCA cases from cohort 1 and analyzed them separately. Surprisingly, using the Youden index-derived cutoffs from the dp-score, we observed a high consistency between NMF subtype and the risk groups. Among the 20 patients, multivariate analysis identified the 4-lipid signature as an independent predictor to detect patients with UCA with rapid growth (OR, 12.91; 95% CI, 1.61–180.5; $p < 0.05$, **Extended Data 1** ***Table S16***). These results showed that the lipid signature had a significant predictive potential to detect patients with UCA with rapid growth (high-risk UCA patients).

Discussion

In the present study, we performed a comprehensive lipidomic analysis of human plasma from HCs, and from patients with UCA and RCA, to investigate altered lipidomic features and identify lipid signatures associated with CAs. We found: 1) The total lipid intensity and most lipid classes from the HC, UCA, and RCA groups decreased significantly ($p < 0.05$). 2) The number of the altered lipids increased and correlated with the severity of the CAs, with low abundance in most altered lipids from all three comparisons (UCA *vs*. HC, RCA *vs*. HC, and RCA *vs*. UCA). 3) TGs were the distinct profile of lipids in plasma from CA samples. 4) The NMF-defined lipidspecific subtypes could not only discriminate between minor (R-I) and severe (R-II) states of patients with RCA, but also predicted slow (U-I) or rapid (U-II) aneurysm growth in patients with UCA. 5) A model incorporating four selected lipid signatures showed good calibration and diagnostic prediction for CA *vs*. HC and UCA *vs*. RCA in both the training and validation clinical cohorts. 6) The four-lipid signature was demonstrated as an independent predictor of discrimination of CA from HC, UCA from RCA, and RCA or UCA subtypes in both the training and validation clinical cohorts.

Decreased plasma lipid levels appeared to correlate negatively with lipid accumulation in the CA wall, as described by Frösen *et al.* [13,14], who revealed that a lipid accumulation was associated with SMCderived foam cell formation, inflammation, mural SMC loss, and CA wall degenerative remodeling, eventually leading to a ruptured CA wall. We hypothesized that lipid accumulation in the CA wall and the normal

artery led to decreased plasma lipid levels. Although Frösen *et al.* found that the plasma total cholesterol and triglyceride levels were often normal, they did not further examine the plasma lipid species and classes/subclasses. Therefore, our results support the theory that lipids and their oxidation products accumulate in the CA wall and lead to the formation, development, and rupture of CA.

In addition, another important result in this study was that TGs represent pivotal lipids associated with CAs. In normal situations, circulating very-low-density lipoprotein (VLDL), intermediate density lipoproteins (IDL) and LDL, which contain TGs, normally flux into and out of the endothelium via transcytosis [23–26]. However, many CA walls have experienced total erosion of their endothelium or do not possess a functionally intact endothelium [7], which increases lipoprotein influx into the vessel wall and causes their accumulation in the CA wall [27]. However, further study is required to determine whether TGs are the most notably altered lipids in CA walls, and how CA formation, development, and rupture are induced by TGs.

In this study, the dp-score, as a diagnostic prediction model, was developed using a four-lipid marker signature. The model could discriminate patients with CA from HCs accurately. The dp-score could differentiate patients with CA with different prognoses effectively and was identified using multivarite analysis as an independent predictive risk factor. The dp-score had a better discriminatory potential than other predictive risk factors (age, gender and hypertension). Moreover, a nomogram was developed comprising the dp-score, age, gender, and hypertension, which showed a slightly superior diagnostic accuracy for CAs in the validation and training cohorts. Thus, the developed nomogram demonstrated a good predictive performance and could be used to predict the prognosis of CA.

Ruptured cerebral aneurysms, which are the most common etiology of nontraumatic subarachnoid hemorrhage (SAH), can cause a catastrophic event with a mortality rate of 25 to 50%, while permanent disability occurs in nearly 50% of survivors; therefore, only approximately one-third of patients who suffer from SAH have a positive outcome [2–5]. In general, the hemorrhage stage is the key factor in determining illness severity in patients with RCA. Patients with considerable SAH are often associated with poor outcomes or disability/mortality. By contrast, patients with minor SAH are often associated with positive outcomes. Using NMF consensusclustering analysis, the patients with RCAs were classified into two major lipid subtypes (R-I and R-II). The patients in R-I exhibited minor hemorrhage and were associated with improved outcomes, while the patients in R-II exhibited considerable hemorrhage and were associated with poor outcomes. The predominant difference between the two subtypes was the difference in lipid intensity. The lipid intensity in RII was lower than that in R-I ($p < 0.05$). while, the 4-lipid signature could act as an independent predictor of distinguish R-I from R-II and detection severe RCA patients in both training and validation clinical cohorts. Therefore, we could distinguish between the two situations or suggest the severity of RCA patients using plasma lipidomics. Furthermore, many catastrophic events, such as disability/mortality, might be rescued if plasma lipidomics or plasma lipid biomarkers could be routinely applied for physical examinations in the future.

With the development of modern CT and MR technology, more and more UCAs can be detected. For patients with UCAs in the clinical settings, we need to definitively resolve whether the patient should undergo treatment or observation. Simply, UCAs could be classified according to their lower or higher risk status. In general, we could discriminate a UCA at lower or higher risk status from its aneurysm characteristics, such as size, shape (regular or irregular), location (bifurcation or sidewall) or aneurysm neck at MRA, CTA, or DSA. In this study, although the lipid intensity in U-II was lower than that in U-I ($p < 0.05$), there were no significant differences in these aneurysm characteristics between the two subgroups, according to NMF consensus-clustering, which was also consistent with our results in the RCA group. Aneurysm rupture did not correlate with size, shape, location, or aneurysm neck in the clinic. Fortunately, we found that U-II subgroup aneurysms were associated with rapid CA progression compared to those in the U-I subgroup. while, the 4-lipid signature demonstrated as an independent predictor of distinguish U-I from U-II and detection UCA patients with rapid growth (high-risk UCA patients) in both cohorts. From this point of view, we might explain the phenomenon observed in the clinic: Why do certain smaller aneurysms rupture easily, while larger aneurysms are more resistant to rupture to some degree. The essential disparity might lie in the difference in lipid accumulation in the CA wall or in the rate of decrease in plasma lipids. Therefore, we hypothesized that the faster the decrease in plasma lipids, the faster the progression in aneurysm growth and ease of rupture.

Currently, except for MRA and/or CTA, there is no other valid approach that can be used for the early diagnosis of UCAs in the clinic. In addition, these techniques are often time-consuming and hospitals with few cases would have limited access, and there are still a large number of cases that could not be detected. Therefore, there is an urgent need for accurate noninvasive biomarkers for the early and differential diagnosis of UCAs. In this study, the 4 lipid signatures not only showed good calibration and diagnostic prediction for CA vs HC and UCA vs RCR, but also demonstrated as an independent predictor of discrimination CA from HC, UCA form RCA, and RCA or UCA subtypes.

Several limitations were associated with this study. First, although we observed specific lipid decreases in plasma, we did not use CA tissue to test whether these decreased lipid species accumulated in the CA wall, because CA tissues are difficult to obtain. Although Frösen *et al.* [13–14] demonstrated that lipids accumulate in all cerebral vasculature and CA walls, they did not indicate which lipids accumulated in the CA wall. Therefore, this detail deserves further investigation. Second, insufficient numbers of participants in the UCA group were subjected to MRA long-term follow-up, and more cases are needed to support our conclusions. Lastly, this study focused on the results observed via lipidomics analysis; however, did not thoroughly investigate the mechanisms or possible signaling pathways. Furthermore, our study did not include aspects related to systemic immunity, which deserves further study.

In summary, comprehensive lipidomic analysis identified decreased lipids as a prominent feature of CAs, and a four-lipid biomarker signature could not only better diagnose and predict UCAs/RCAs from HCs, but also predicted subtypes of patients with severe RCA or high-risk UCA. On the one hand, these results highlight a possible key role of plasma lipidomics to support the theory of lipid accumulation in the CA wall. On the other hand, the results highlight the favorable predictive capability of the four-lipid biomarker

signature as a diagnostic predictive potential tool to assess the prognosis of CA. Although lipidomic data of the CA wall are lacking and long-term follow-up with more case are needed, our data provides important biological insights and clear clinical implications for the future.

Materials And Methods

Study design and patient recruitment

This study was approved by the Human Ethics Committee of Shanghai Jiao Tong University Affiliated Sixth People's Hospital and Renji Hospital, Shanghai Jiao Tong University, School of Medicine, and informed consent was obtained directly from the patients or their first-degree relatives of unconscious subjects before the start of the experiment. A total of 1388 patients without intervention were enrolled at Shanghai Jiao Tong University Affiliated Sixth People's Hospital (952 cases, 2014.03–2019.05) and Renji Hospital, Shanghai Jiao Tong University School of Medicine (436 cases, 2017.10–2019.08). Patients (n = 360, cohort 1) from the Shanghai Sixth People's Hospital were recruited for comprehensive lipidomic analysis, and 180 cases (cohort 2), from Renji Hospital were applied for validation.

A case-control study with a matched sex and age design was used. Samples were selected (n = 540) from the 1388 participants with available blood samples according to the following order: We first divided these patients into three groups according to their diagnostic status (HC, UCA, and RCA); and then four subgroups according to age [≤ 45 (n = 135), 46 to 55 (n = 135), 56 to 65 (n = 135), and > 65 years (n = 135)] were classified in each group; finally, men (n = 216) and women (n = 324), with a ratio of 1:1.5, were allocated to each subgroup. Blood samples were taken from an arm vein or from the femoral artery with no intravenous transfusion. Peripheral blood samples (10 mL) were collected from each patient into EDTA-vacutainers (BD, Franklin Lakes, NJ, USA). Plasma was centrifuged at 3000 × *g* for 10 min to remove cells within three hours and then stored at −80 °C until use.

Patients with CA diagnosed using computed tomography angiography (CTA), magnetic resonance angiography (MRA), and/or digit subtraction angiography (DSA), and patients without CA (diagnosed by MRA) with normal liver and renal function, and electrolyte levels served as a comparison group. Patients were referred for these procedures for numerous reasons, including acute processes, such as subarachnoid hemorrhage (SAH) and intracranial hemorrhage, as well as for nonacute indications to rule out cerebrovascular diseases, such as headache, dizziness, or no symptoms. Patients with abnormal liver functions caused by a malignant tumor, hepatitis, hepatic cirrhosis, liver function failure, and other hepatic diseases were excluded from the study.

The collected baseline data included clinical information, biochemical characteristics, and the demographics of all participants.

Image acquisition and image review

MRA, CTA, and/or DSA examinations were described previously and are not presented here (6). The aneurysm type was classified as saccular and fusiform. Aneurysm size was recorded as the maximum 2D angiographic or MRA dimension: (1) < 3 mm, (2) 3–5 mm, (3) > 5–10 mm, or (4) > 10 mm. The number of aneurysms was classified into two groups: Single and multiple aneurysms. Aneurysm locations were grouped into four categories: The anterior communicating artery (ACA), the middle cerebral artery (MCA), the internal carotid artery (ICA), and the vertebral and basal artery system (VBAS), or into bifurcation and sidewall aneurysms. Aneurysm shape was classified as either regular or irregular (with daughter sac or lobulated). The aneurysm neck was defined as either narrow or wide (≥ 4 mm or fundus:neck ratio ≤ 2). Aneurysm growth was defined as an aneurysm that increased by > 1 mm in maximum diameter during follow-ups, as compared with the initial examination.

Three observers, who were highly experienced in neurointerventional radiology and had previously tested the application common-standard interpretation techniques, were blinded to all clinical, CTA, MRA, and DSA results. They analyzed all datasets independently on an offline-workstation from multiple on-screen viewing angles. In the event of interobserver discrepancies in the detection of intracranial aneurysms, consensus was achieved or a majority decision was obtained.

Sample preparation and lipid extraction

MS-grade methanol, MS-grade acetonitrile, and HPLC-grade 2-propanol were purchased from Thermo Fisher (Janssen pharmaceuticalaan 3a2440 Geel-Belgium). HPLC-grade formic acid and HPLC-grade ammonium formate were purchased from Sigma-Aldrich (St. Louis, MO, USA). Lipids were extracted according to the methyl-tert-butyl ether (MTBE) method. Briefly, plasma samples were thawed at 4 °C, and 100 µL of each sample was mixed with 240 µL of cold methanol and 200 µL of water to remove the protein. Next, 800 µL of MTBE was added, and the mixture was subjected to ultrasound for 20 min at 4 °C, followed by incubation at room temperature for 30 min. The solution was centrifuged at 14000 × *g* for 15 min at 10 °C, and the upper organic solvent layer was obtained and dried under nitrogen. For LC-MS analysis, the samples were re-dissolved and vortexed in 200 µL of an isopropanol solution. To monitor the stability and repeatability of the instrument analyses, quality control (QC) samples were prepared by pooling each sample, and these were analyzed together with the other samples. The sample queue was randomly tested to remove bias.

LC-MS method for lipid analysis

Reverse phase chromatography was selected for LC separation using a CSH C18 column (1.7 µm, 2.1 mm× 100 mm, Waters, Milford, MA, USA). The lipid extracts were re-dissolved in 200 µL of 90% isopropanol/ acetonitrile, centrifuged at 14000 × *g* for 15 min, and finally, 3 µL of sample was injected. Solvent A was acetonitrile–water (6:4, v/v) with 0.1% formic acid and 0.1 mM ammonium formate, while solvent B was acetonitrile–isopropanol (1:9, v/v) with 0.1% formic acid and 0.1 mM ammonium formate. The initial mobile phase was 30% solvent B at a flow rate of 300 µL/min. It was held for 2 min, and then linearly increased to 100% solvent B in 23 min, followed by equilibration at 5% solvent B for 10 min.

Mass spectra were acquired by Q Exactive Plus in positive and negative mode. Electrospray ionization (ESI) parameters were optimized and preset for all measurements as follows: Source temperature, 300 °C; Capillary Temp, 350 °C. In positive ion mode, the ion spray voltage was set at 3000 V, the S-Lens RF level was set at 50%, and the scan range of the instrument was set at m/z 200–1800. In negative ion mode, the ion spray voltage was set at -2500 V, the S-Lens RF level was set at 60%, and the scan range of the instrument was set at m/z 250–1800.

Identification by lipid Search

LipidSearch software (Thermo Scientific™) was employed to conduct lipid identification and data processing on the raw data, which included peak extraction, lipid identification, peak alignment, and quantification. This software contains MS2 & MS3 databases of 8 categories, 300 subclasses, and about 1.7 million lipid molecules.

Statistical analysis

Normalization of lipid data

For large-scale lipidomics studies, we used the support vector regression (SVR) normalization method to normalize lipid data to effectively remove the intra-batch and inter-batch variations in the LC-MS analysis. In brief, the intensities of 360 (120 healthy, 120 Non-SAH, and 120 SAH) samples were extracted from the lipid data, resulting in a 1312 × 360 lipid-expression matrix. Then, QC-SVR, implemented in the R/Bioconductor package, MetNormalizer, was used to normalize the expression matrix. For subsequent quantitative analyses, the normalized intensities were log2-transformed. In addition, the samples were removed when the missing values was more than 30%. The remaining missing values were imputed by the nearest 10 neighbors using the k-Nearest Neighbor algorithm.

Lipid difference analysis

The data was first log2 scaled before multivariate data analysis (MVDA), computed with the ropls R package. This package implements unsupervised principal component analysis (PCA) analysis, with supervised partial least squares discriminant analysis (PLS-DA) and orthogonal partial least squares discriminant analysis (OPLS-DA) based on the original, NIPALS-based, versions of the algorithms. Using this package, the R2 and Q2 quality metrics, the score and orthogonal distances, the permutation diagnostics, as well as the variable importance for projection (VIP) values could be calculated. Permutation testing was performed 200 times. Score plots, loadings, and permutation plots were generated with the calculated results using R. The variables were standardized (mean-centered and Pareto scaled, which is the same as the Par scaling method in software SIMCA) prior to model building. The ropls package is available from the Bioconductor repository. Univariate statistical analysis includes Student's *t*-test and variance multiple analysis.

Lipidomic subtype identification in aneurysm patients: To identify the lipidomic subtypes in the lipid expression matrix from the 240 aneurysm samples, we used the NMF v.0.21.0 consensus cluster method

from the R package. NMF is a machine learning method that can efficiently identify distinct molecular patterns and molecular classifications. For each lipid in the samples, we first calculated the coefficient of variation, which was used produce a descending order of ranked metabolites. NMF v.0.20.6 in R v.3.6.1 unsupervised consensus-clustering was then used to analyze the top 30% most-variant lipids. The nsNMF algorithm was carried out using 469 iterations for the clustering runs and 200 iterations for the rank survey. The average silhouette width for clustering solutions between 2 and 6 clusters and the profiles of the cophenetic score were used to select the preferred cluster result. From the lipidomic data, the silhouette width, rank survey profiles of the cophenetic score, together with the consensus membership heat maps, suggested a two-subtype solution for patients with aneurysm.

The categorical basic and demographic characteristic variables are shown as numbers and percentages, and c2 test was used for their comparisons. Continuous variables, shown as the mean (± SD), if normally distributed, were compared using an unpaired *t*-test. Non-normally distributed data are presented as the median (interquartile range), and differences were determined using one-way analysis of variance (ANOVA) and a Wilcoxon rank sum text. Statistical significance was indicated by a p value £ 0.05.

To select biomarkers, least absolute shrinkage and selection operator (LASSO) was performed using the "glmnet" package and package caret was used to perform random forest algorithms. Subsequently, the generalized linear model (glm, regressions) was constructed to analyze the biomarkers. The "car" package was used to calculated the VIP values. The "pROC" package was used to plot the ROC curve. The "rms" package was used to construct the nomogram and produce the calibration plots. the was conducted using the "HLtest.R." was used to perform the Hosmer–Lemeshow test, and "ggDCA.R." was used to perform the DCA.

In addition, to build the cd-score, we fitted a logistic regression model. The performance of the cd-score–based classifier was assessed using a ROC curve, which provided assigned cases to high- and low-risk groups using Youden index-derived cutoff thresholds from the four-lipid signature model. The Wilcoxon test was used to examine the distribution of the cd-score between clinical categories. To compare the discriminatory performance of the dp-score, age, sex, hypertension, and other factors, ROC was used. To determine the effects of potential risk factors, multivariate logistic regression analysis was used. R software, version 3.6.1 was used to perform all the analyses.

Note that cohort 1 and cohort 2 were analyzed independently (without being normalized together) for comprehensive lipidomic profile analysis, and the training cohort (cohort 1) and validation cohort (cohort 2) were normalized together for biomarker analysis.

References

1. Meyers PM, et al. Reporting standards for endovascular repair of saccular intracranial cerebral aneurysms. Stroke. **40**, e366-79 (2009).

2. Wiebers DO, et al, International Study of Unruptured Intracranial Aneurysms Investigators. Unruptured intracranial aneurysms: natural history, clinical outcome, and risks of surgical and endovascular treatment. Lancet. **362**,103–110 (2003).
3. Brisman JL, Song JK, Newell DW. Cerebral aneurysms. N Engl J Med **355**,928–939(2006).
4. van Gijn J, Kerr RS, Rinkel GJ. Subarachnoid haemorrhage. Lancet. **369**,306–318(2009).
5. Vlak MH, Algra A, Brandenburg R, Rinkel GJ. Prevalence of unruptured intracranial aneurysms, with emphasis on sex, age, comorbidity, country, and time period: a systematic review and meta-analysis. Lancet Neurol. **10**,626–636 (2011).
6. Li MH, et al. Prevalence of Unruptured Cerebral Aneurysms in Chinese Adults Aged 35 to 75 Years: A Cross-sectional Study. Ann Intern Med. **159**,514–521(2013).
7. Frösen J, et al. Saccular intracranial aneurysm: pathology and mechanisms. Acta Neuropathol. **123**,773 – 86(2012).
8. Kataoka K, et al. Structural fragility and inflammatory response of ruptured cerebral aneurysms. A comparative study between ruptured and unruptured cerebral aneurysms. Stroke. **30**,1396–1401(1999).
9. Frosen J, et al.Remodeling of saccular cerebral artery aneurysm wall is associated with rupture: histological analysis of 24 unruptured and 42 ruptured cases. Stroke. **35**,2287–2293(2004).
10. Tulamo R, et al. Complement activation associates with saccular cerebral artery aneurysm wall degeneration and rupture. Neurosurgery. **59**,1069–1076(2006).
11. Kosierkiewicz TA, Factor SM, Dickson DW. Immunocytochemical studies of atherosclerotic lesions of cerebral berry aneurysms. J Neuropathol Exp Neurol. **53**,399–406(1994).
12. Tulamo R, et al. Complement system becomes activated by the classical pathway in intracranial aneurysm walls. Lab Invest. **90**,168 – 79(2010).
13. Frösen J, et al. Lipid accumulation, lipid oxidation, and low plasma levels of acquired antibodies against oxidized lipids associate with degeneration and rupture of the intracranial aneurysm wall. Acta Neuropathol Commun.**1**,71(2013).
14. Ollikainen E, et al. Smooth Muscle Cell Foam Cell Formation, Apolipoproteins, and ABCA1 in Intracranial Aneurysms: Implications for Lipid Accumulation as a Promoter of Aneurysm Wall Rupture. J Neuropathol Exp Neurol. **75**,689 – 99 (2016).
15. Ollikainen E, et al. Mast cells, neovascularization, and microhemorrhages are associated with saccular intracranial artery aneurysm wall remodeling. J Neuropathol Exp Neurol. **73**,855 – 64(2014).
16. Razquin C, et al. Plasma Lipidomic Profiling and Risk of Type 2 Diabetes in the PREDIMED Trial. Diabetes Care. **41**,2617–2624(2018).
17. Meikle PJ, et al. Plasma lipidomic analysis of stable and unstable coronary artery disease. Arterioscler Thromb Vasc Biol. **31**,2723–2732(2011).
18. Stegemann C, et al. Lipidomics profiling and risk of cardiovascular disease in the prospective population-based Bruneck study. Circulation. **129**,1821–1831(2014).

19. Cancer Genome Atlas Network. Comprehensive molecular portraits of human breast tumours. Nature. **490**,61–70(2012).
20. Jiang Y, et al; Chinese Human Proteome Project (CNHPP) Consortium. Proteomics identifies new therapeutic targets of early-stage hepatocellular carcinoma. Nature. **567**,257–261(2019).
21. Frontera JA, et al. Prediction of symptomatic vasospasm after subarachnoid hemorrhage: the modified fisher scale. Neurosurgery. **59**,21 – 7(2009).
22. Sun L, et al; China Kadoorie Biobank Collaborative Group; International Steering Committee; International Co-ordinating Centre, Oxford; National Co-ordinating Centre, Beijing; Regional Co-ordinating Centres. Causal associations of blood lipids with risk of ischemic stroke and intracerebral hemorrhage in Chinese adults. Nat Med. **25**,569–574(2019).
23. Kyle JE, et al. Plasma lipidome reveals critical illness and recovery from human Ebola virus disease. Proc Natl Acad Sci U S A. 116,3919–3928(2016).
24. Armstrong SM, et al. A novel assay uncovers an unexpected role for SR-BI in LDL transcytosis. Cardiovasc Res. **108**,268 – 77(2015).
25. Fogelstrand P, Boren J. Retention of atherogenic lipoproteins in the artery wall and its role in atherogenesis. Nutr Metab Cardiovasc Dis. **22**,1–7(2012).
26. Huang L, et al. SR-B1 drives endothelial cell LDL transcytosis via DOCK4 to promote atherosclerosis. Nature. **569**,565–569. (2019).
27. Annema W, von Eckardstein A, Kovanen PT. HDL and atherothrombotic vascular disease. Handb Exp Pharmacol. **224**,369–403(2015).

Figures

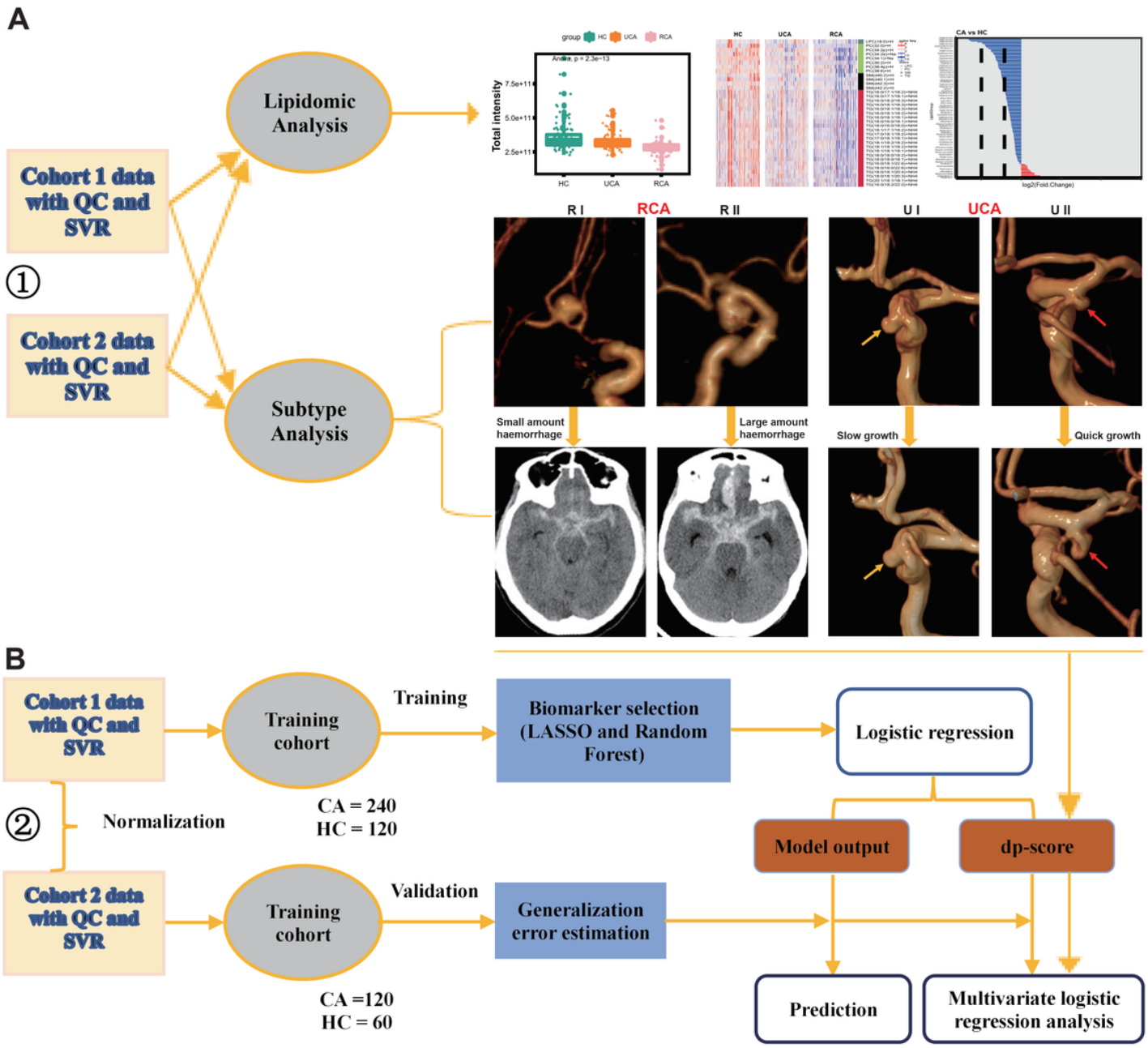

Figure 1

Brief study designs. (A) step 1, workflow for lipidomic analysis and subtype analysis (RI and RII for RCA, UI and UII for UCA). (B) step 2, workflow for building the diagnostic prediction model for CA vs HC and RCA vs UCA, and in addition to lipid signature with diagnostic prediction (dp) score for CA vs HC, UCA vs RCA, and RCA or UCA subtypes. Note: QC = Quality control; SVR = Support vector regression; HC = Health control; UCA = Unruptured cerebral aneurysm; RCA = Ruptured cerebral aneurysm.

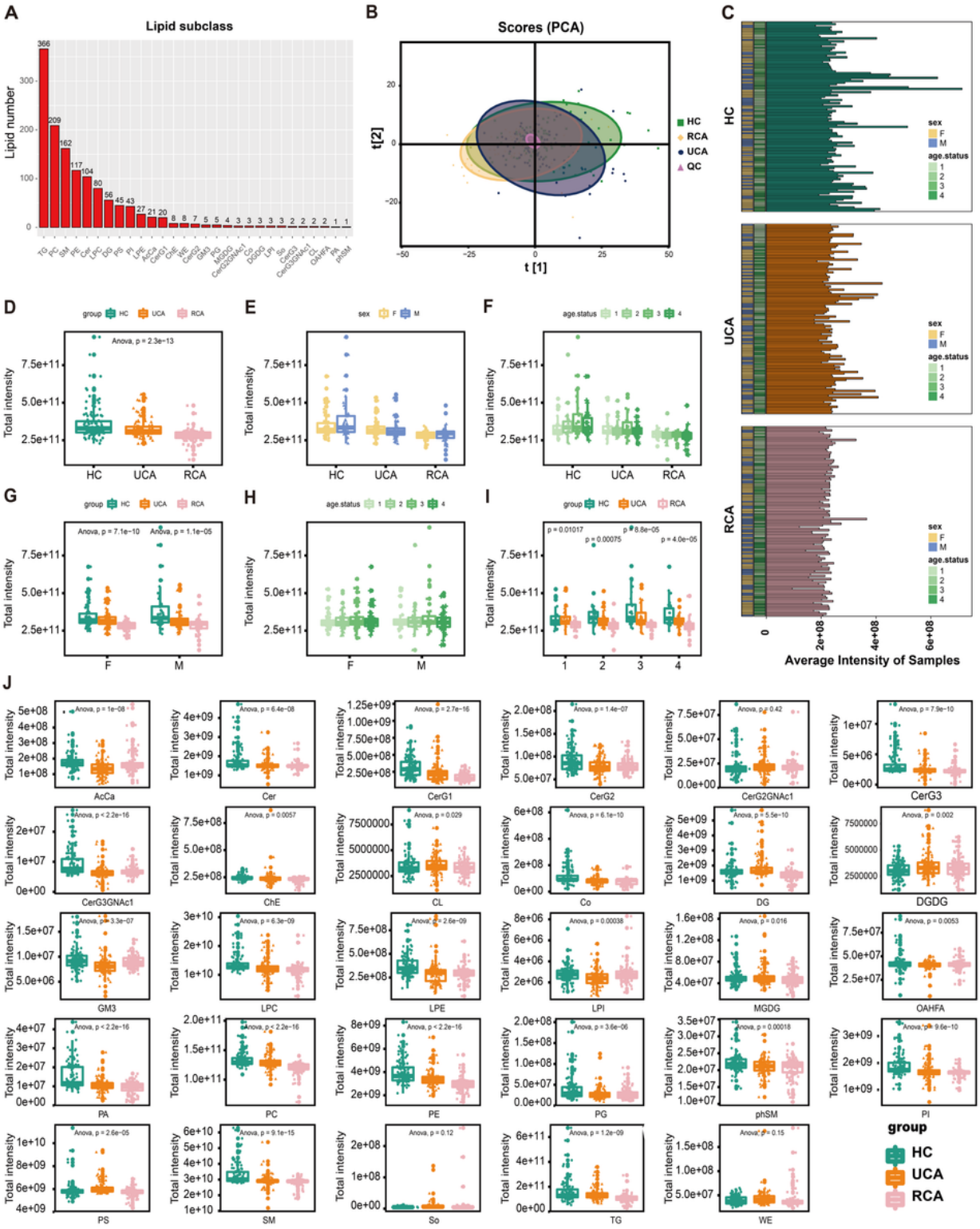

Figure 2

Overview of the analysis of lipids and lipid subclass intensity in the three groups (A) LC-MS detected 1312 lipids covering 29 subclasses in all three groups, in which TG was the most abundant lipid in all three groups, followed by PC, SM, PE and Cer. (B) Principal component analysis (PCA) scores of HCs (thin green), patients with UCA (blue), patients with RCA (egg color), and QC samples (calamus color). (C) Total lipid intensity of every sample in the three groups accompanied by sex and age data. (D-I) Comparisons

of the total lipid intensity in the three groups, with or without sex and/or age data. Age status: 1 indicates ≤ 45, 2 indicates 46 to 55, 3 indicates 56 to 65, and 4 indicates > 65 years. (J) Comparisons of the total lipid intensity in 29 lipid classes among the three groups. In the box plots, and the interquartile range is represented by the box and the median is represented by the middle bar; dots show all data values. The two-sided Wilcoxon test or ANOVA test was used to calculate the p values, which are shown on top of the boxes.

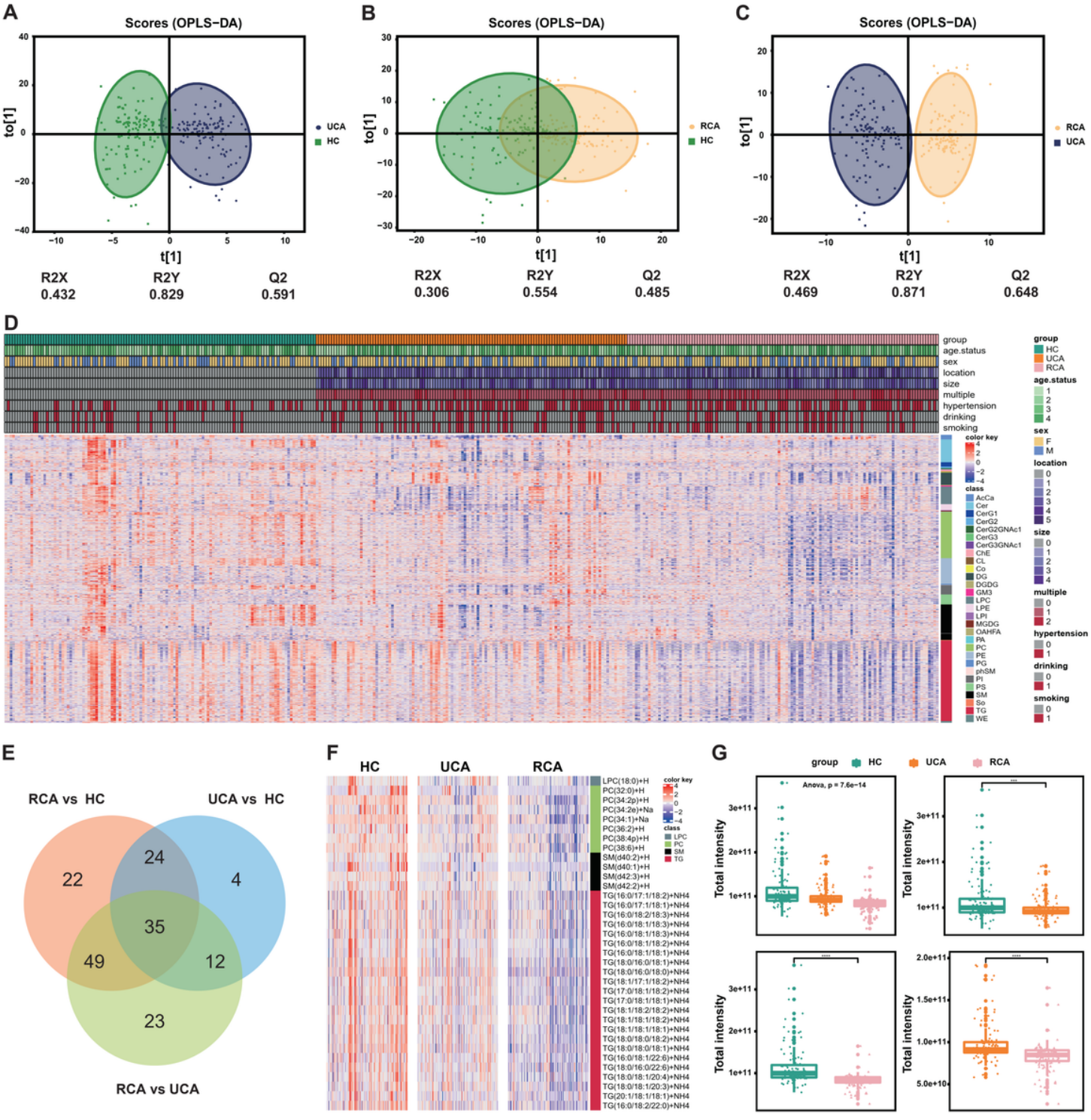

Figure 3

Plasma lipidomic profiling of HCs, UCAs, and RCAs (A-C) Orthogonal partial least-squares discriminant analysis (OPLS-DA) score plot of the comparison between the UCA and HC groups, RCA and HC groups, and RCA and UCA groups. (D) A heatmap showing all lipids relative abundance. On the right, clinical information and lipid subclass related to these signature lipids are shown. (E) Venn diagram displaying 35 differentially abundant lipids, as biomarker candidates from the three comparisons. (F) A heatmap showing the relative levels of these 35 lipid profiles when comparing UCA to HC, RCA to HC, and RCA to UCA. (G) Box plots of the 35 lipids among the three groups and in each of the two comparisons. The two-sided Wilcoxon test or ANOVA test were used to calculate the p values and are shown on top of the boxes. *$p < 0.05$, **$p < 0.01$, ***$p < 0.001$.

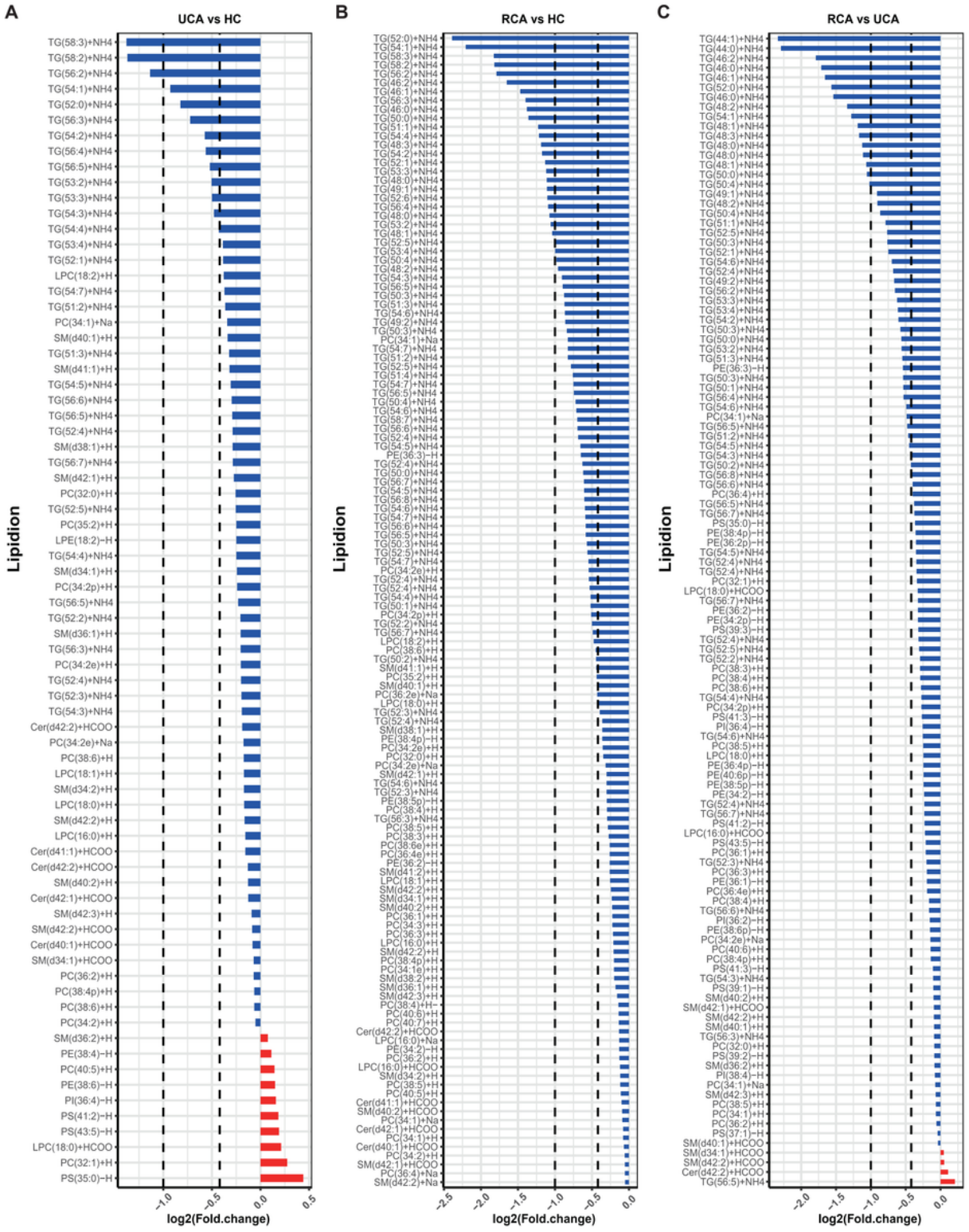

Figure 4

TGs were the distinct profile of lipids in patients with CAs (A) The bar chart shows 65 differential lipids are downregulated (blue bar) and 10 are upregulated (red bar) from the comparisons of UCA vs HC. 13 lipids are significantly decreased (inner dashed line) and only 3 TG lipids showed a less than 0.5-fold decrease (outer dashed line). (B) The bar chart displays all 130 differential lipids are downregulated (blue bar) from the comparisons of RCA vs HC. 75 lipids are significantly decreased (inner dashed line) and 24

lipids shows a less than 0.5-fold decrease (outer dashed line). All the 24 lipids are TGs. (C) The bar chart exhibits 115 differential lipids are downregulated (blue bar) and 4 are upregulated (red bar) from the comparisons of RCA vs UCA. 46 lipids are significantly decreased (inner dashed line) and 16 lipids shows a less than 0.5-fold decrease (outer dashed line). All the 16 lipids are TGs.

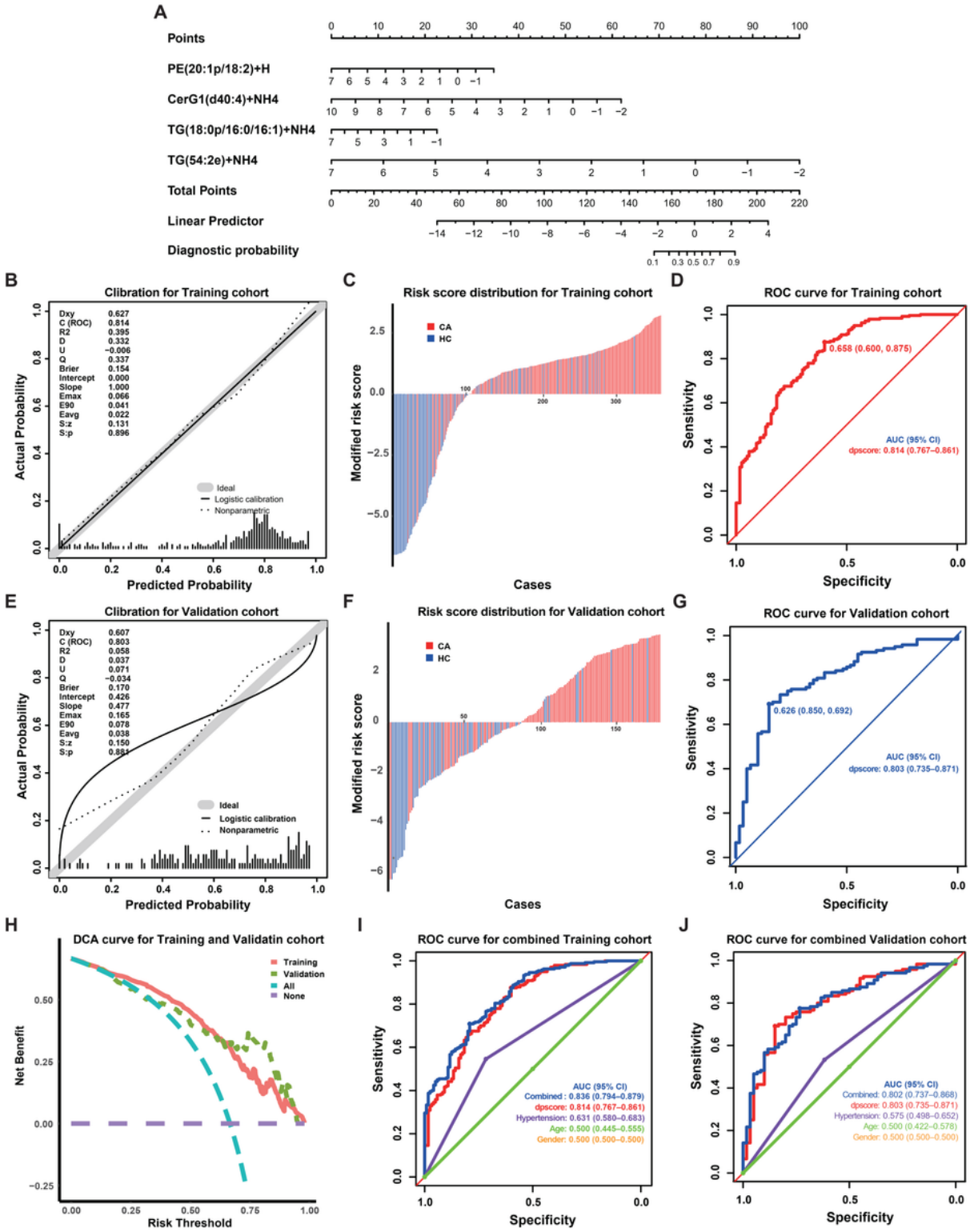

Figure 5

Lipid-based diagnostic prediction model for CA vs. HC (A) Developed lipid nomogram in the training cohort incorporating four lipid signatures: PE (20:1p/18:2)+H, CerG1 (d40:4)+NH4, TG (18:0p/16:0/16:1)+NH4, and TG (54:2e)+NH4. (B) Training cohort: Calibration curve of the lipidomic nomogram. Notes: Nomogram calibration incorporated the agreement between the predicted diagnostic probability of CA vs. HC and the observed outcomes of CA vs. HC. (C) Assessment of nomogram's predictive accuracy for the training cohort for the four-lipid signature using ROC curves (CA = 240, HC = 120, AUC = 0.814). (D) Plot of the training cohort's risk score distribution. Subtraction of the individual risk score from the Youden index value in the risk model produced the modified risk score. (E) Validation cohort: Calibration curve of the lipidomic nomogram. (F) Assessment of nomogram's predictive accuracy for the validation cohort for the four-lipid signature using ROC curves (CA = 120, HC = 60, AUC = 0.803). (G) Plot of the validation cohort's risk score distribution. (H) Comparison the clinical utility of the International Task Force Consensus Statement algorithm (blue dotted line) with our model (red and green dotted line) using DCA. Plotting the net benefit (y-axis) for a range of potential thresholds based on the diagnostic probability (x-axis) was used to compare the clinical utility of all strategies. Among all the potential thresholds (5–95%), our model for the training and validation cohorts showed the highest net benefit. For the potential thresholds (35– 90%), our model for the test cohort demonstrated the highest net benefit. This suggested that the developed model would produce a high weighted balance of positive versus negative diagnosis of CAs, regardless of the clinically preferred risk threshold. (I, J) A ROC curve of the combination model (4-lipid signature, age, sex, and hypertension) in the (I) training cohort (CA = 240, HC = 120, AUC 0.836) and (J) validation cohort (CA = 120, HC = 60, AUC 0.802). DCA, Decision curve analysis.

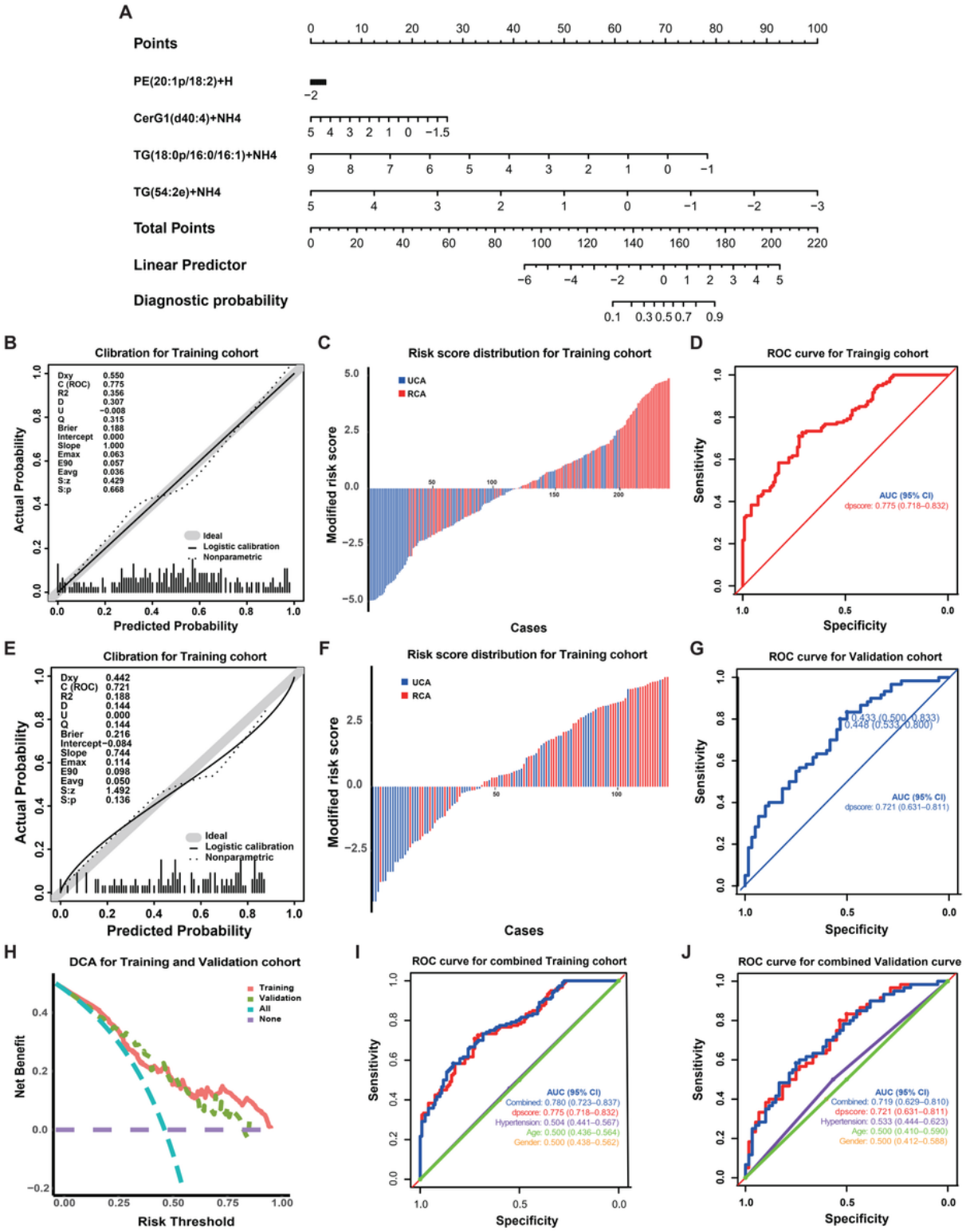

Figure 6

Lipid-based diagnostic prediction model for UCA vs. RCA (A) The developed lipid nomogram in the training cohort incorporating four lipid signatures: PE (20:1p/18:2)+H, CerG1 (d40:4)+NH4, TG (18:0p/16:0/16:1)+NH4, and TG (54:2e)+NH4. (B) Calibration curve of the lipidomic nomogram of UCA vs. RCA in the training cohort. (C) ROC curves were used to determine the nomogram's predictive accuracy for the 4-lipid signature in the training cohort (UCA = 120, RCA = 120, AUC = 0.775). (D) Training cohort:

Risk score distribution plot. Subtraction of the individual risk score from the Youden index value in the risk model produced the modified risk score. (E) Validation cohort: Calibration curve of the lipidomic nomogram. (F) ROC curves were used to determine the nomogram's predictive accuracy for the 4-lipid signature in the validation cohort (UCA = 60, RCA = 60, AUC = 0.721). (G) Risk score distribution plot in the training cohort. (H) Comparison the clinical utility of the International Task Force Consensus Statement algorithm (blue dotted line) with our model (red and green dotted line) using DCA. Among all the potential thresholds (5–95%), our model for the training and validation cohorts showed the highest net benefit. For the potential thresholds (20–85%), suggesting that the developed model produce the high weighted balance of positive versus negative diagnosis of UCAs or RCAs, regardless of the clinically preferred risk threshold. (I, J) A ROC curve of the combination model (four-lipid signature, age, sex, and hypertension) in the (I) training cohort (UCA = 120, RCA = 120, AUC 0.78) and (J) validation cohort (UCA = 60, RCA = 60, AUC 0.719). DCA, Decision curve analysis.

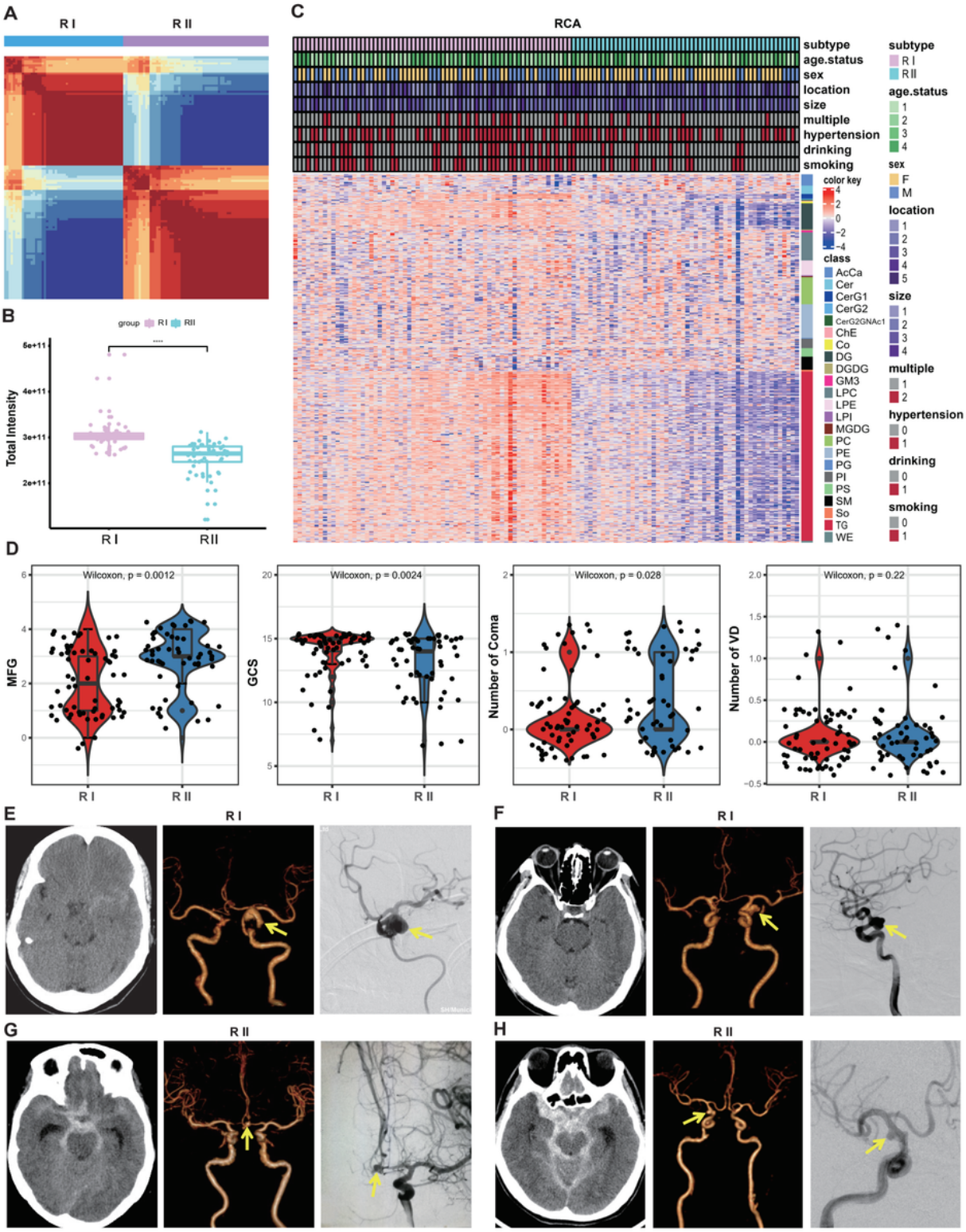

Figure 7

Lipid-defined specific subtypes discriminate between minor and severe states of patients with RCA (A) Lipidomic profiling analyzed using NMF consensus-clustering identifies two lipid subtypes (RCA samples, n = 120): R-I (light magenta, n = 65) and R-II (light cyan, n = 55). (B) Box plot showing the comparison of the total lipid intensity between R-I and R-II. (C) Heatmap depicting the relative abundance of the lipid intensities of the two subtypes. The associations of lipid subtypes with clinical characteristics are

annotated in the middle panel. The lipid classes are denoted on the right. (D) Box plot showing the differences in modified fisher grade (MFD), Glasgow Coma Scale (GCS), the frequency of Coma, and the number of ventricular drainage (VD) between the two subtypes. (E) Ruptured aneurysm (arrow) in the R-I subtype on the left C7 segment of the ICA (size: 12.6 × 10.5) in a 51-year-old female patient with an MFD of 1 and a GCS of 15 before embolization. (F) Ruptured aneurysm (arrow) in the R-I subtype on the left C7 segment of the ICA (size: 10.1 × 9.8) in a 52-year-old male patient with an MFD of 1 and a GCS of 15 before embolization. (G) Ruptured aneurysm (arrow) in the R-II subtype on the anterior communicating artery (size: 2.4 × 2.3) in a 60-year-old female patient with an MFD of 4 and a GSC of 10 before embolization. (H) Ruptured aneurysm (arrow) in the R-II subtype on the right C7 segment of the ICA (size: 1.5 × 1.2) in a 41-year-old male patient with an MFD of 3 and a GSC of 14 before embolization.

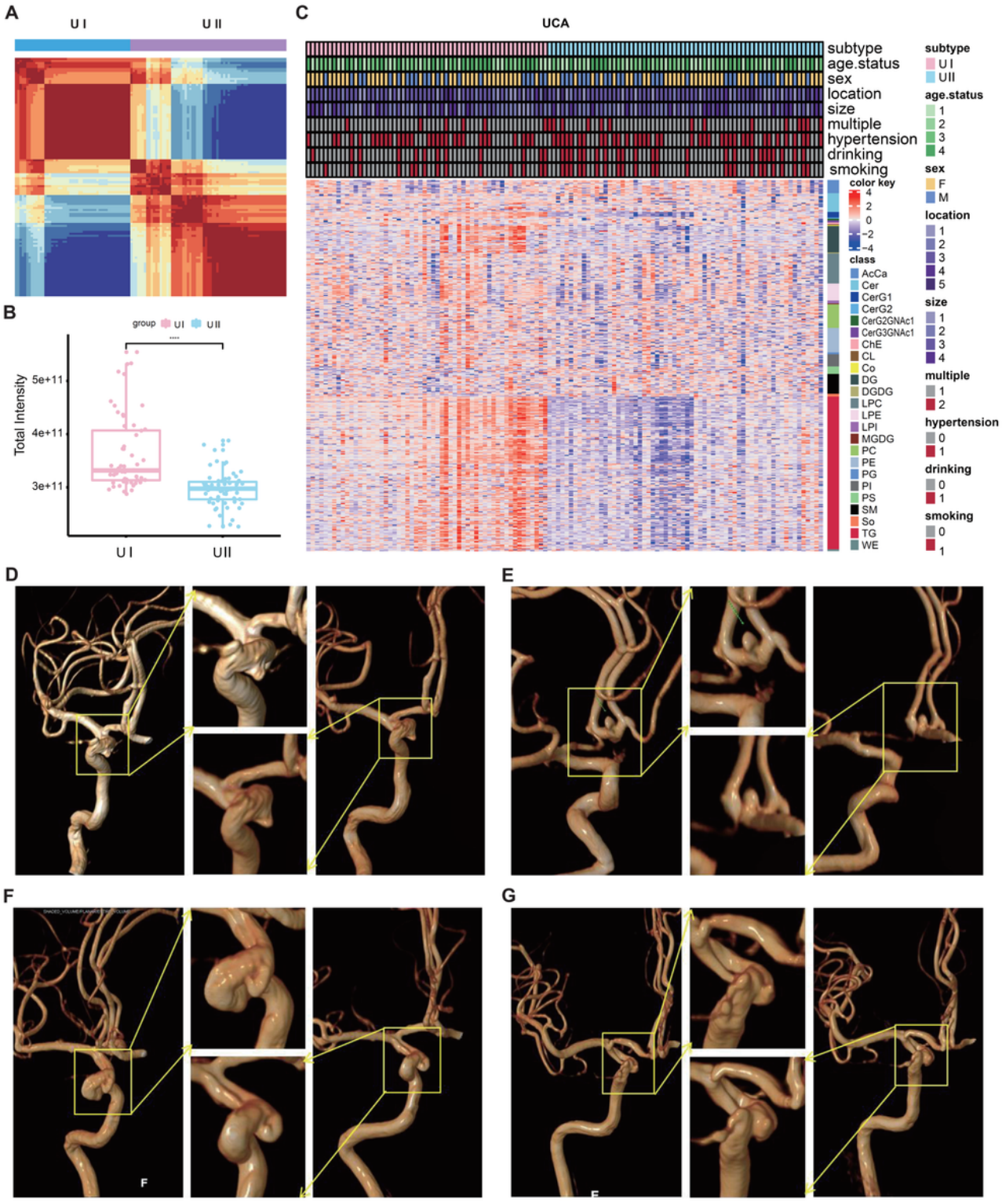

Figure 8

UCA subtypes predict slow or rapid aneurysm growth (A) Lipidomic profiling analyzed using NMF consensus-clustering identifies two lipid subtypes (UCA samples, n = 120): U-I (pink, n = 54) and U-II (light blue, n = 66). (B) Box plot showing the comparison of the total lipid intensity between U-I and U-II. (C) Heatmap depicting the relative abundance (intensity) of the lipids of the two subtypes. The middle panel shows the clinical characteristics with lipid subtypes. The lipid class is denoted on the right. (D) A case in

the U-I group. Three-dimensional time-of-flight magnetic resonance angiography (MRA) reveals a small aneurysm (arrow) of the C6 segment of internal carotid artery. MRA at 7-year follow-up displays that the aneurism (arrow) has not grown. (E) Another case in the U-I group. Three-dimensional time-of-flight MRA reveals a small aneurysm (arrow) of the anterior communicating artery. MRA at 7-year follow-up also displays that the aneurism (arrow) has not grown. (F) A case in the U-II group. Three-dimensional time-of-flight MRA image reveals a small aneurysm (arrow) of the C6 segment of the internal carotid artery. MRA at 7-year follow-up shows an increase in the size of the aneurysm (arrow). (G) Another case in the U-II group. Three-dimensional time-of-flight MRA image reveals a small aneurysm (arrow) of the C6 segment of the internal carotid artery in U-II. MRA at 7-year follow-up shows an increase the size of the aneurysm (arrow).

Supplementary Files

This is a list of supplementary files associated with this preprint. Click to download.

- SupplementaryMaterials.docx
- SupplementaryMaterials.docx
- rsflat.pdf